Scanning Microscopy

Volume 1993
Number 7 *Physics of Generation and Detection of Signals Used for Microcharacterization*
Article 3

1993

A Few Steps Towards a More Quantitative Understanding of Contrast in the Scanning Electron Microscope

F. Hasselbach
Universität Tübingen, Germany

U. Maier
Universität Tübingen, Germany

Scanning Microscopy Supplement 7, 1993 (Pages 21-32) 08921-953X/93$5.00+.25
Scanning Microscopy International, Chicago (AMF O'Hare), IL 60666 USA

A FEW STEPS TOWARDS A MORE QUANTITATIVE UNDERSTANDING OF CONTRAST IN THE SCANNING ELECTRON MICROSCOPE

F. Hasselbach* and U. Maier

Institut für Angewandte Physik der Universität Tübingen, Tübingen, Germany

Abstract

The interaction volume of the electron beam with the specimen in a scanning electron microscope (SEM) is a highly complex function of the surface structure of the specimen, its chemical composition and the energy of the scanning electron beam. The video signals formed by secondary electrons (SE) or backscattered electrons (BSE) reflect this complexity insofar as they may contain not only information of the interior of the pixel which has just been scanned and its neighborhood, but may depend on surface details hundreds of microns apart from the impinging point of the electron beam. This leads to artifacts in scanning electron micrographs, e.g., edge brightening. The knowledge of the spatial distribution of the current density of the BSE and SE released by the impinging beam are the key for a more quantitative understanding of contrasts in scanning electron micrographs.

In a first step, our emission microscopic method to visualize these distributions has been improved by substituting a photographic registration method by a charged couple device (CCD) densitometer. The resolution of our present densitometer (256 grey levels) is not sufficient to record the full dynamic range of the SE current density distributions. However, this will be possible in the near future with a state of the art CCD-camera and a 14 bit image processing system.

Key Words: Scanning electron microscopy, contrast formation with secondary and backscattered electrons, interaction- and information volume, spatial distributions of secondary electrons, dependence of spatial distributions on topography, topography contrast, edge brightening, compositional contrast, electron emission microscope, CCD-imaging.

*Address for correspondence:
Franz Hasselbach
Institut für Angewandte Physik
Auf der Morgenstelle 12
D 7400 Tübingen, Germany
Phone Number: 7071/296 328
FAX Number: 7071/295 400

Introduction

The most widely used signals for image formation in the scanning electron microscope (SEM) are those formed by secondary electrons (SE) and by backscattered electrons (BSE). Secondary electrons are produced by the impinging primaries and the scattered electrons along the whole path of the electrons through the specimen. Only secondaries that are generated in distances to the surface smaller than the typical escape depth of a few nm leave the specimen surface and eventually contribute to the SE video signal. The secondaries produced by the impinging primaries when penetrating through the specimen surface are usually classified as SE1 and contain information with a resolution limit corresponding roughly to the diameter of the scanning beam. In contrast to these SE1, the source of secondaries generated by the backscattered electrons when leaving the surface of the specimen again, is not highly localized but rather extended. The size of the source of this second class of SE, well known as SE2, is at least of the order of the electron range in the specimen. In general, it is even more extended as we will see later. The backscattered electrons, which leave the specimen surface, may hit the walls of the specimen chamber of the SEM generating there a third component of SE, the SE3, containing, via a variation of the backscattering coefficient η, mainly compositional information about the specimen.

Interaction- and Information Volume

Interaction- and information volume of BSE

The interaction volume is determined by the sum of all trajectories of the scattered electrons in the specimen, while the information volume is defined as that volume which is visible to the detector of the SEM. In a scintillation detector for BSE, e.g., the low-energetic BSE are stopped in the metallization layer of the scintillator and do not contribute to the video signal. The information volume is consequently smaller than the interaction volume. When an energy dispersive (low-loss-) detector is used for BSE detection, the information volume and, in turn, the resolution in BSE micrographs can be chosen

Symbol Table

α:	exit angle of backscattered electrons to the surface normal
β:	secondary yield enhancement factor
γ:	secondary emission coefficient
η:	backscattering coefficient
δ_{av}:	average secondary emission coefficient
η_{av}:	average backscattering coefficient
C:	contrast of two adjacent pixels
C^*:	"single pixel contrast"
C_{x*}:	single pixel contrast of pixel no. x
C^{**}:	single pixel contrast at low magnification
E_o:	energy of primary electrons
I_x:	intensity in pixel no. x

at will, just by selecting an appropriate energy window for the BSE and thus determining the part of the BSE contributing to the video signal. A large information volume corresponds to a large exit area of the BSE over which the signal of BSE is averaged. This leads to a reduced spatial resolution in the micrographs. Topographic details considerably smaller than the information volume which is accepted by the detector are not resolved. Since the information volume varies for the different types of detectors, the resolution of BSE micrographs depends on the type of BSE-detector used and decreases in the following succession: low-loss detector [30, 31], scintillation detector [8, 25], converted BSE to SE detector [20]. The interaction- and information volume of the BSE strongly depends on the beam energy, the atomic number, weight and density of the specimen, the tilt angle of the primary beam to the surface normal, the take-off angle of the BSE and last, but not least, on the surface structure of the specimen.

Interaction- and information volume of SE

The production of secondary electrons takes place along the whole path of the scattered electrons through the specimen, yet only the secondaries produced in a subsurface layer corresponding to the mean free path of the secondaries (of less than one or two nm) are able to escape and contribute to the SE1 and SE2 signals. Thus, while the interaction volume of the secondaries is, cum grano salis, the same as that of the primary beam, the volume where the secondaries which reach the detector come from is given by the intersection of a very thin subsurface layer, about one escape depth wide, with the interaction volume. In other words, only secondaries produced in this thin subsurface layer contribute to the SE video signal in the SEM. However, the information which is transported by the SE2 type secondaries is a mixture of information contained in the BSE signal and some low resolution information about the surface topography: the total number of the SE2 depends not only on the total number of backscattered electrons emerging from the interaction volume, but also strongly on the surface topography, since the secondary emission coefficient δ is proportional to $1/\cos\alpha$, where α means the local exit angle of the BSE to the surface normal. However, the dependence of the SE2 current on the surface topography is varies slowly compared to the SE1 signal. This is due to the fact that, apart from low-voltage SEM, (**1**) the SE2 emerge from a large surface area compared to the area of the impinging primary probe. Consequently, surface topographic information is averaged over the comparatively large exit area of the BSE; and (**2**) the SE2 signal contains subsurface information to a depth of about half the range of the primaries.

Highly resolved topographic information is contained only in the current of secondaries which is produced in the interaction area of the primary probe with the surface of the specimen, the SE1 type secondaries. Let us bear in mind that a very small fraction of SE1 is produced by those backscattered electrons which emerge from the specimen surface **inside** the primary probe area. The ratio of the number of secondaries produced by these backscattered electrons to the total number of secondaries emerging from **inside** this area (we define both as belonging to the SE1 secondaries) is approaching zero with decreasing diameter of the impinging primary probe, i.e., in the limiting case of high resolution, the SE1 signal contains purely surface topographic information (we consider for the moment a specimen detail with a constant secondary emission coefficient δ, i.e., contrast is due exclusively to the inclination of the surface with respect to the direction of the primary beam) with an information depth given by the mean free path of the secondary electrons.

Contrast Formation in BSE- and SE-Micrographs

In the present paper, we are not interested in contrast formation by special detection methods for the SE and BSE electrons, e.g., by multiple detector arrangements and signal mixing [5, 6, 16], by signal processing [23] or by crystal orientation contrast. We focus our interest on the total BSE, SE1, and SE2 currents emerging from the specimen surface and the information that can be extracted from these currents as they are detected by conventionally used BSE and SE detectors. We do not take into account the influence of the SE3-type secondaries since these can be suppressed by taking suitable measures. In order to understand contrast formation with BSE and SE quantitatively, it is necessary to

quantitatively know the exact current density distributions of the BSE, the SE1 and the SE2 released by a highly focused impinging electron probe, favorably a probe of negligible diameter (δ-probe). From this knowledge, and knowing which of these electrons contribute to the video signal produced by the detector, the corresponding total intensities I_1 and I_2 in two adjacent pixels and, in turn, the contrast can be calculated according to its well known definition:

$$C = (I_1 - I_2)/(I_1 + I_2). \quad (1)$$

The main purpose of this paper is to demonstrate that our combination of a scanning electron microscope with an emission microscope, together with state of the art image detection and processing, is to our knowledge the only possibility at hand to measure the current densities of SE1, SE2 and, indirectly, of the BSE electrons spatially resolved.

Contrast formation in BSE micrographs

In BSE-micrographs, contrast is mainly formed (1) by the monotonic increase of the backscattering coefficient η with the atomic number [22] in the information volume seen by the detector (the information volume is depending on the inclination of the specimen surface, the solid angle subtended by the detector and the energy spread of the electrons contributing to the video signal); and (2) by shadow casting effects of the surface structures of the specimen in the direction to the detector. The best visibility of atomic number contrast is achieved when the width of the energy window of the accepted BSE is about $0.7E_0$ - E_0, where E_0 is the energy of the primary beam [21]. The total current of BSE contains subsurface information to a depth of about half the range of the primaries and topographic information averaged over a surface area with a diameter of about the range of the primaries. As already mentioned, the current of BSE accepted by the detector is usually smaller than the total one and so is the actual information volume.

Figure 1. Electron-optical setup.

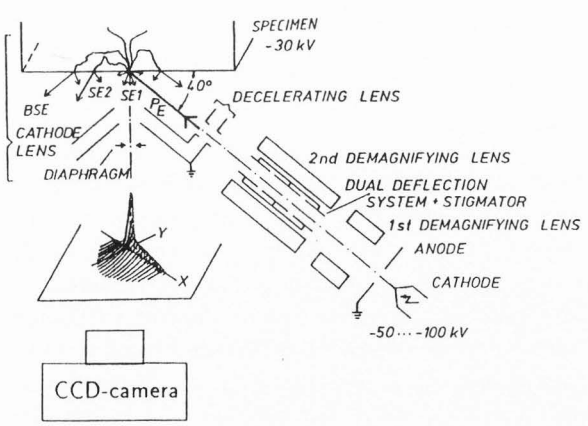

Contrast formation in SE micrographs

Contrast in SE-mode micrographs is mainly influenced by the ratio of the number SE1/SE2 secondaries since conventional secondary electron detectors cannot discriminate between SE1 and SE2 secondaries and form the video signal out of the sum of both. The SE2 signal is generated by reemerging BSE in the relatively large surface area where the BSE leave the specimen surface. It is similar or even larger in amplitude than that of the SE1 since the bulk backscattering coefficient η is typically of the order of 10-50%, and the secondary yield is enhanced by a factor $\beta \sim 1.5...5$ [2, 3, 12, 27, 28] for the re-emerging BSE. Thus, the total secondary yield δ can be written as:

$$\delta = SE1 + SE2 = SE1(1 + \beta\eta). \quad (2)$$

The β-value is an important quantity in SE imaging because its value determines, together with the backscattering coefficient η, the ratio SE1/SE2, i.e., the fractional content of high resolution SE1 electrons in the video signal. Experimental data on β in the literature are at least partly contradictory. Our experimental values of about 2 for energies in the range of 20-70 keV [12] corroborate the low values of Drescher *et al.* [7]. For low energies between 1-10 keV, the experimental values of the order of 4-6 [1, 4, 18, 26] are in good agreement, e.g., with the results of Monte Carlo calculations of Luo and Joy [19]. Hopefully, the experimental technique which is described in the present work will be a step forward in measuring β more precisely.

The SE2 current normally varies slowly in time, compared to the SE1 signal, and acts as a superimposed background signal in highly resolved micrographs. We will see later that the spatial distribution and the number of SE2 can be a very complicated function of the topography of the specimen surface.

Experimental Technique for Measuring Spatial Distributions of BSE, SE1 and SE2

Electron optics

The exact knowledge of the spatial distributions of the BSE, SE1 and SE2 is an indispensable prerequisite for understanding contrast in scanning electron micrographs. In order to measure these distributions quantitatively, we combined a scanning electron microscope with an electron emission microscope [9, 10, 11] (Figure 1). The scanning electron microscopical column, given on the right hand side of Figure 1, forms a spot of 0.3-1.0 μm in diameter on the specimen surface at energies of

Table 1. Characteristics of the CCD-Camera.

	TV- CCD-camera with Thompson-CSF 7863 sensor
number of pixels	384 (horizontal) x 288 (vertical)
form of pixels	quadratic
size of pixels	23 x 23 μm
size of sensitive area	6.624 x 8.832 mm
dark signal non-uniformity	0.1% of the saturation output voltage
photo response non-uniformity of pixels	$\leq$ 3%
dynamic range	$\approx$ 1 : 2000
on-chip integration time	20 ms - 20 min
readout period	20 ms

20-70 keV. The SE1 and SE2 released by the impinging primaries and the BSE are accelerated by the high electric field in front of the specimen surface which is generated by the potential applied to the specimen with respect to the anode and the focusing electrode of the cathode lens. This lens projects a magnified, spatially resolved image of the distribution of the SE1 + SE2 on the fluorescent screen of a highly linear and highly sensitive charged coupled device- (CCD-) image recording system. The cathode lens uses secondary electrons only for image formation. All electrons emitted from the surface of the specimen with energies greater than about 2 eV are cut off in the back focal plane by the 30 μm diaphragm. BSE are not focused by the cathode lens in the image plane of the SE due to their high energy and energy spread. Details of the electron optical setup and results obtained with the photographic registration may be found elsewhere [e.g., 9, 10, 11, 12, 15]. Since the current density of the SE1 and SE2 is spatially varying at least by two or three orders of magnitude, special precautions were necessary to register these distributions photographically. This traditional method has been replaced recently by an electronic detection method with high dynamic range and linearity.

Highly linear recording of two-dimensional current density distributions

Quantitative electron microscopy urgently needs quantitative electron detection methods. In the past, the only recording medium was the photographic plate with its many deficiencies, e.g., (**1**) low dynamic range, due to saturation effects at high exposure levels and granularity, i.e., in photographic emulsions, the sensitive particles tend to clump together. This produces the well-known granularity which hides features that are small or have low contrast. Both effects lead to a poor detection quantum efficiency (DQE); (**2**) poor geometric stability. This means that during the developing process, the relative distances of certain structural features may change; and (**3**) the photometric accuracy of photographic emulsions depends on the developing process. Photographic emulsions are not linear detection devices even when material only from the same batch of photographic emulsion is used in an experiment. Each film roll must be individually calibrated if a high accuracy is necessary. This is a laborious process which is not very accurate in itself.

The very limited dynamic range and the poor photometric accuracy of the photographic recording method were the main reasons that we were looking for an electronic method with less or none of the deficiencies given in the last paragraph.

The most promising electronic device, which has become available in the last decade, is the CCD-imaging device. The value of its quantum efficiency reaches up to 70% compared to 20% for photocathodes or a few per cent for photographic emulsions and for the unaided eye. The low noise level, its corresponding enormous dynamic range of about 1:5000 for standard CCD-chips and up to 1:50000 for specially selected ones and its inherent linearity are unique and unsurpassed by other detection methods. The data of our CCD-camera are given in Table 1. The dark signal non-uniformity of 0.1% of the maximal output voltage and the photo response non-uniformity of $\leq$ 3% must be corrected by image processing in order to realize the large dynamic range. In the spatial distributions presented in this paper, we could not take full advantage of these excellent data of the CCD-sensor since the frame store of the image processing system which was at our disposal for these experiments resolved 256 grey levels only.

A schematic diagram of the CCD-detection and image processing system which replaces the photographic plates is given in Figure 2. The electrons excite a P 20 phosphor screen which is deposited on a fiberoptic faceplate. The fiberoptic faceplate acts as a vacuum interface and transmits the image via the fiberoptic entrance of the CCD-camera directly to the photo sensitive pixels of the CCD-chip. The fiber optic transfer of the image is superior to lens optical coupling in two respects: (**1**) It is more efficient in light transfer; and (**2**) there is no vignetting, and it is geometrically stable.

The integration time of a picture on the CCD-chip can be chosen in the range of 20 milliseconds (TV-frequency) to about 20 minutes. The readout period is 20 ms. The CCD-array can be cooled by Peltier elements down to about -10° centigrade. This cooling is necessary in order to reduce the thermally generated

electrons in the pixels of the CCD-sensor at long integration times. These electrons are the limiting factor for the dynamic range of the camera. Our present image processing system limits the useful dynamic range to 256 grey levels (8 bit) as mentioned previously. The dynamic range of the cooled CCD-sensor is about 20 times that value. It is remarkable that, even with the CCD-sensor at room temperature, the dynamic range of the camera exceeds 8 bit for integration times of up to 4 s.

In order to take full advantage of the system in the future, a slow scan CCD-camera in combination with a 14 bit image processing system will be indispensable because the fast readout period of our camera limits its dynamic range to about 1:2000 at TV-frequency due to crosstalk of the fast timing signals in the camera electronics.

The image processing system consists of an 8 bit analog to digital (A/D) converter, a frame store for 2 pictures with 512 x 512 pixels, a personal computer, a look-up table, a digital to analog (D/A) converter, a monitor and a laser printer for documentation. By choosing a logarithmic look-up table, the scale representing the intensity is changed in such a way that it is expanded in the low-intensity parts and compressed in the high intensity parts.

Figure 3 gives, on the left-hand side, a linear and, on the right-hand side, a logarithmic plot of the spatial distribution of the SE1 + SE2 current density from a polished Si surface released by a focused beam of diameter 1 μm. The SE2 current density distribution becomes clearly visible when the scale of low-intensity parts is expanded logarithmically. Since the SE current density distribution is proportional to the BSE current density distribution for flat specimens of low atomic number [14] (β and η correlate the SE and BSE currents), our experimentally obtained SE2 distributions may be compared to theoretically evaluated BSE distributions, e.g., to the Monte Carlo calculations of Tholomier *et al.* [29]. Our experimental parameters (angle of incidence, energy of primary electrons) differ from those used by Tholomier *et al.* for their calculations; therefore, we can only state qualitative consistency.

Spatial Distributions of SE, the Grey Levels of Single Pixels, "Single Pixel Contrast"

In a SEM, the image is usually observed on the fluorescent screen of a high resolution CRT tube. Each

Figure 2. CCD-detection and image processing system.

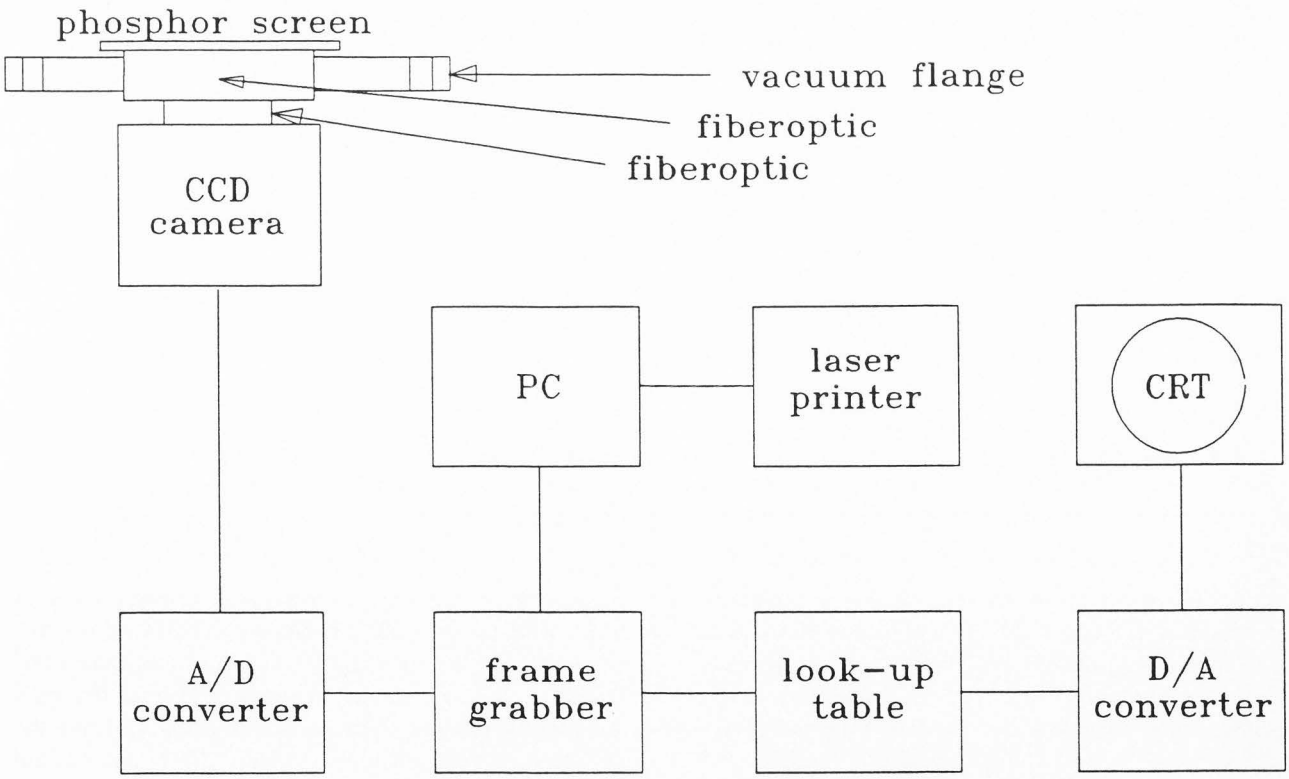

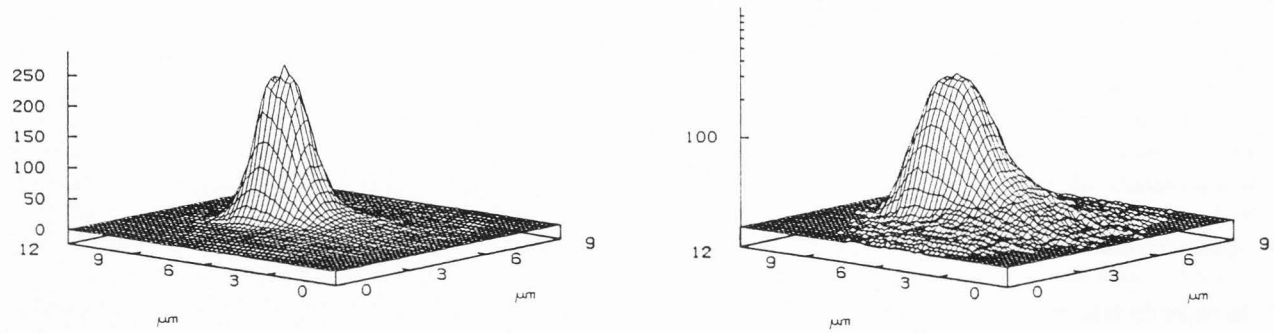

Figure 3. Spatial distributions of secondary electrons released by a fine impinging primary probe (1 μm in diameter) of 30 keV of energy from a polished silicon wafer. The angle of incidence was 50° to the surface normal. On the left-hand side, a linear look-up table was chosen for the intensity and, on the right-hand side, a logarithmic one.

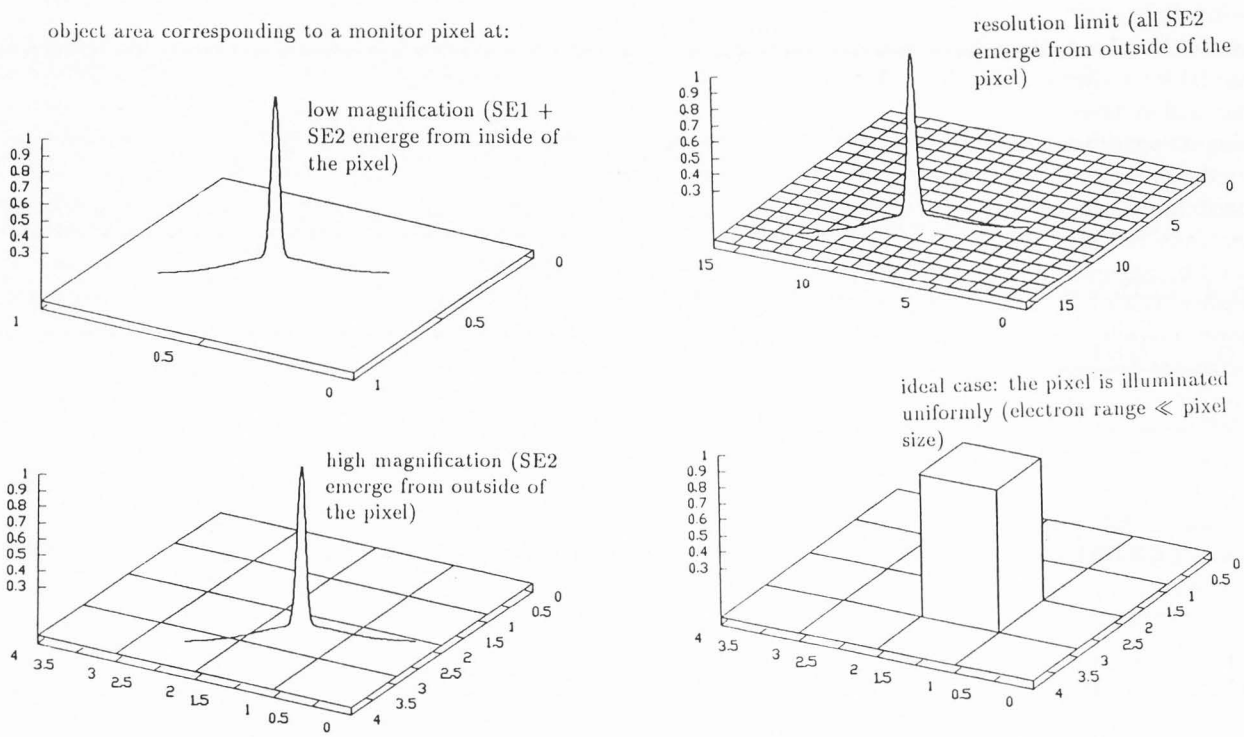

Figure 4. Escaping area of the SE2 as a function of magnification in a scanning electron micrograph. Only at low magnification do the SE2 carry useful information. Ideally, a shaped beam (constant current over the pixel area) of low-energy electrons should impinge on the surface of the specimen.

---

pixel of the image on its screen, which we assume to have the dimensions 0.1 x 0.1 mm^2, is correlated with a correspondingly smaller pixel on the specimen surface, e.g., at a magnification of 100, its dimensions on the specimen surface are 1 x 1 μm^2. These dimensions correspond to the resolution limit in the micrograph. We expect that the grey level of this pixel gives information of the highest accuracy when (**1**) a primary electron beam with constant current density is incident over the whole area of the pixel and (**2**) the range (determined by the energy) of the primary electrons is so small that only a negligible number of backscattered electrons leave the specimen surface outside the pixel. If (1) and (2) are taken for granted, the current of SE1 + SE2 or BSE

electrons leaving the pixel in question characterizes the average secondary emission factor δ_{av} or the average backscattering coefficient η_{av} in this pixel. On these premises, we expect to observe a micrograph of the specimen surface with the highest possible fidelity. In reality, these conditions are fulfilled to a rough degree in low-voltage scanning electron micrographs but not at all in conventional scanning electron micrographs. This is most easily understood (Figure 4) when we consider the two limiting cases of imaging at low magnification and imaging at the resolution limit of a conventional SEM. At low magnification, the electron probe is usually focused into a smaller spot than the pixel area, i.e., the current of SE1 electrons does not represent the δ_{av} in the whole pixel but the δ in a small part of this pixel. Additionally, the spatial distribution of the BSE and the SE2 current density are not constant inside the pixel area and may, depending on the magnification and the energy of the primaries, extend beyond the pixel area. The total BSE and SE2 current does not characterize the η_{av} inside of the pixel. At high magnification, the current density distribution of the focused spot on the specimen surface is likewise not constant inside of the pixel area but is of Gaussian distribution. Nearly all BSE and SE2 leave the specimen surface, in this limiting case, outside the pixel which has just been scanned. In conclusion, in neither the case of low nor high magnification do scanning electron micrographs contain quantitative information in the sense that the grey levels in the pixels represent average information on δ or η of the pixel just scanned.

"Single pixel contrast"

We define this contrast as the fraction of the secondary electron signal of a single pixel that carries useful information at the resolution limit [12] to the total secondary current:

$$C^* = SE1/(SE1 + SE2). \quad (3)$$

It characterizes the signal to background ratio in each pixel at the resolution limit and neither depends, within the limits of error of our experimental investigation for flat specimens of Si, Ge and Ag [12], on the energy of the primaries (20-70 keV) nor on the material. This result is interesting insofar as the signal to background ratio in the scanning electron micrographs of homogeneous specimens and, in turn, the contrast and resolution that can be achieved do not depend on the atomic number of the specimen involved. This becomes clear when we keep in mind the relation between conventional contrast C and single pixel contrast C_1^* and C_2^* of two adjacent pixels:

$$C = (I_1 - I_2)/(I_1 + I_2) = \tfrac{1}{2}(C_1^* - C_2^*). \quad (4)$$

We obtained these results for flat specimens a few years ago with the old photographic registration method. The fact that the spatial distributions of the SE1 and SE2 showed to be Gaussian-distributed to a high degree of accuracy was very important for the evaluation of the total currents of SE1 and SE2. These currents were obtained by simply integrating the distributions analytically.

With decreasing magnification $SE1/(SE1 + SE2) = C^{**}$ is no longer constant but increases due to the fact that the fraction of secondaries which are released outside the pixel previously scanned decreases. It depends not only on the magnification but also strongly on the specimen structure. For rough specimens, the number of SE2 increases drastically because the interaction volume of the scattered electrons is cut by steps, edges and surface structures (Figure 5). Then, more scattered electrons leave the specimen surface as backscattered electrons. These BSE may reenter the specimen and release secondaries far from the impinging point of the primary beam, forming a second, important contribution to the SE2-type secondary current. This second component of SE2 is largely responsible for the well known edge brightening effect. We observed the emission sites of both types of SE2 for steps, oblique planes and edges for the first time in 1976 [13]. Monte Carlo simulations of such distributions of SE and BSE have been published, e.g., by Reimer [24] and Kotera [17].

Figure 5. In rough specimens, the pear-shaped interaction volume of the scattered electrons is cut by edges, leading to an increased emission of SE2 and BSE. Two components of SE2 may be distinguished: (1) the SE2 released by the emerging scattered electrons and (2) the SE2 released by scattered electrons penetrating into the specimen surface again, far from the point of incidence of the primary beam.

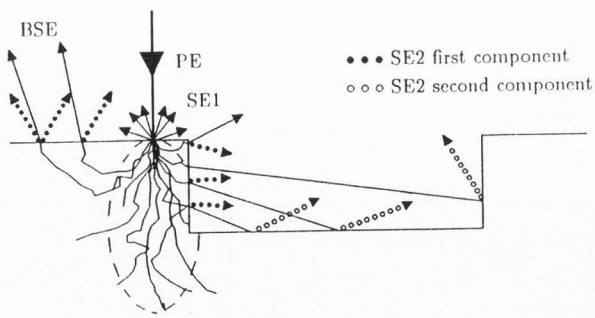

Spatial Distributions of SE1 + SE2 Released from Complicated Specimen Structures

The combination of our emission microscopical method with a CCD-camera and an on-line image processing system gives us a unique possibility to quantitatively record and store spatial distributions of secondary electrons with an extremely high dynamic range. This can be done for any surface structure regardless of how complicated it is. Furthermore, it is possible, for example, to quantitatively record the spatial distributions of two adjacent pixels on two pages of our image processing system, subtract and add the data of these two spatial distributions and divide the results. In this way, we can quantitatively compute the contrast of two adjacent pixels by image processing.

We cannot present quantitative results of current density distributions released from steps and other complicated specimen structures at the moment because (**1**) the dynamic range of our present CCD-densitometer system is limited to 256 grey levels, which is insufficient for this application, and (**2**) alterations of the electron optics of the instrument and the computer system are in progress and not yet finished. Anyway, Figures 6 and 7 give an idea of the potential of the new method. As an example, we digitized photographically recorded current density distributions by using our CCD-camera and image processing system. In Figure 6a, an emission micrograph of a scan over quadratic steps of gold on an aluminium substrate is shown. The steps were 30 nm high, and the energy of the primary beam was 40 keV. In Figure 6b, a part of the digitized intensity distribution of the secondaries released by the line scan is presented. Figure 7 schematically shows a focused electron beam impinging on the specimen described above (Figure 6) as well as the digitized intensity distribution of the secondaries. The component of SE2 released by scattered electrons reimpinging on the specimen surface far from the impinging point of the primary electron probe is clearly visible in the intensity distribution (Figure 7b). The contribution of this second class of SE2 to the total SE2 yield is substantial. The current density

---

Figure 6. (**a**) Emission micrograph (recorded on a photographic plate) of the spatial distribution of SE1 + SE2 released by the scanning electron beam. (**b**) Digitized intensity distribution of SE.

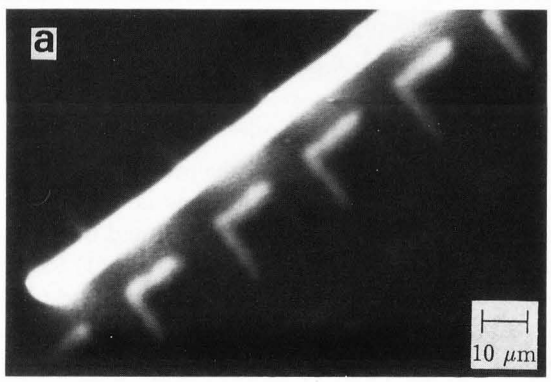

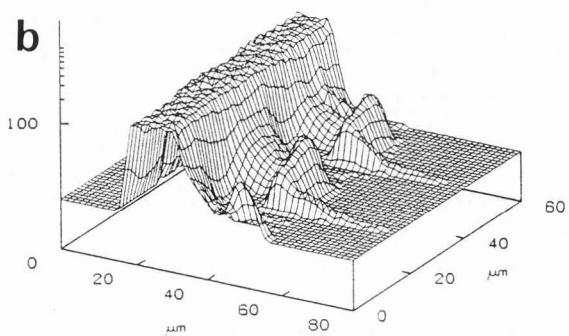

Figure 7. (**a**) Schematic diagram of the same specimen as in Figure 6 with a focused electron beam impinging near the edge of one of the quadratic steps. (**b**) Digitized intensity distribution of SE released by the focused electron beam.

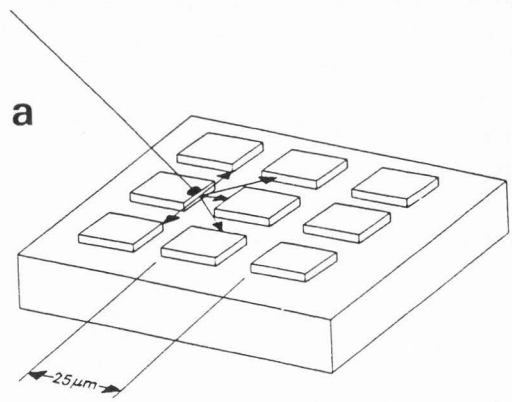

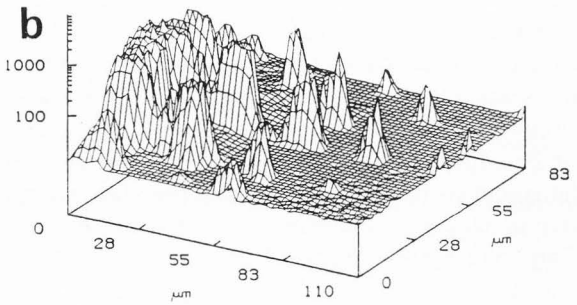

released is very low; however, the total yield is large due to the large emission area.

Conclusions

In order to quantitatively understand contrast in scanning electron micrographs, quantitative knowledge of the spatial distributions of SE1 and SE2 is indispensable. The emission microscopical method to visualize these distributions in combination with an up-to-date CCD-data aquisition system of high dynamic range and linearity, both exceeding 3 orders of magnitude, enables us to quantitatively record the spatial distributions of secondaries released from complex specimen structures. The potential of the method will become evident when a slow scan CCD-camera combined with an image processing system with 14 bit in depth will be at hand. Then, the results of the numerous Monte Carlo calculations [17, 24] can be checked experimentally for the first time.

References

[1] Bindi R, Lanteri H, Rostaing P, Keller P (1980) Theoretical efficiency of backscattered electrons in secondary electron emission from aluminium. J. Phys. D: Appl. Phys. **13**, 2351-2361.

[2] Bronshtein IM, Denisov SS (1967) Secondary electron emission of aluminium and nickel obliquely incident primary electrons. Sov. Phys.-Solid State **9**, 731-732.

[3] Bronshtein IM, Dolinin VA (1968) Secondary electron emission (SEE) of solids at large angles of incidence of the primary beam. Sov. Phys.-Solid State **9**, 2133-2140.

[4] Bronshtein IM, Fraiman BS (1961) Inelastic scattering of electrons and secondary emission from certain metals and semiconductors. Sov. Phys.-Solid State, **3**, 1188-1196.

[5] Buczkowski A, Hejna J, Radzimski Z (1988) Signal mixing technique for backscattered electrons in the scanning electron microscope. Scanning Microscopy **2**, 633-638.

[6] Crewe AV, Lin PSD (1976) The use of backscattered electrons for imaging purposes in a scanning electron microscope. Ultramicroscopy **1**, 231-238.

[7] Drescher H, Reimer L, Seidel H (1970) Rückstreukoeffizient und Sekundärelektronenausbeute von 10-100 keV-Elektronen und Beziehungen zur Raster-Elektronenmikroskopie. (Backscattering coefficients and secondary electron yield of 10 to 100 keV-electrons and relations to scanning electron microscopy.) Z. Angew. Physik **29**, 331-336.

[8] Everhart TE, Thornley RFM (1960) Wideband detector for microampere low-energy electron currents. J. Sci. Instr. **37**, 246-248.

[9] Hasselbach F (1971) Untersuchung der Verbreiterung von fokussierten Elektronenstrahlen durch Streuung in dünnen und dicken Objekten mit dem Elektronenemissionsmikroskop. (Investigation of the broadening of focused electron beams by scattering in films and bulk specimens with the electron emission microscope.) 15. Tagung für Elektronenmikroskopie 1971 (Karlsruhe). Mikroskopie **28**, 352 (abstract).

[10] Hasselbach F (1973) Messung der Ortsverteilung von gestreuten Elektronen in Durchstrahlung und Reflexion im Elektronenemissionsmikroskop. (Measurement of spatial current density distributions of scattered electrons in transmission and reflection with an electron emission microscope.) Ph.D. Thesis, Universität of Tübingen.

[11] Hasselbach F (1988) The emission microscope, a valuable tool for investigating the fundamentals of the scanning electron microscope. Scanning Microscopy **2**, 41-56.

[12] Hasselbach F, Krauss H-R (1988) Backscattered electrons and their influence on contrast in the scanning electron microscope. Scanning Microscopy **2**, 1947-1956.

[13] Hasselbach F, Rieke U (1976) Emission microscopical investigation of the edge brightening effect in scanning electron microscopy. 6th. European Congress on Electron Microscopy (Jerusalem). Vol. I. TAL International Publishing Company, Jerusalem, Israel, 296-298.

[14] Hasselbach F, Rieke U (1978) Emission microscopical investigation of the proximity effect in electron beam lithography. 9th International Congress on Electron Microscopy (Toronto). Vol. I. Sturgess JM, Kalnins VI, Ottensmeyer FP, Simon GT (eds.), Microscopical Society of Canada, Toronto, Ontario, 166-167.

[15] Hasselbach F, Rieke U (1982) Spatial distribution of secondaries released by backscattered electrons in silicon and gold for 20-70 keV primary energy. Proc. 10th International Congress on Electron Microscopy (Hamburg). Vol. I. Deutsche Gesellschaft für Elektronenmikroskopie e. V., Berlin, Germany, 253-254.

[16] Hejna J, Reimer L (1987) Backscattered electron multidetector systems for improved quantitative topographic contrast. Scanning **9**, 162-172.

[17] Kotera M, Kishida H, Suga H (1990) Monte Carlo simulation of secondary electrons in solids and its application for scanning electron microscopy. Scanning Microscopy Supplement **4**, 111-126.

[18] Lanteri H, Richard C, Bindi R, Keller P (1975) Determination experimentale de l'éfficacité des électrons rétrodiffusés dans l'émission électronique secondaire de Au et Al. (Experimental determination of the influence

of backscattered electrons on secondary electron emission in gold and aluminum.) Thin Solid Films **27**, 301-310.

[19] Luo S, Joy DC (1990) Monte Carlo calculations of secondary emission. Scanning Microscopy Supplement **4**, 127-146.

[20] Moll SH, Healey F, Sullivan B, Johnson W (1978) A high efficiency, non-directional backscattered electron detection mode for the SEM. Scanning Electron Microscopy **1978**;I, SEM Inc., AMF O'Hare, 303-310.

[21] Newbury DE, Joy DC, Echlin P, Fiori CE, Goldstein JI (eds.) (1987) Advanced Scanning Electron Microscopy and X-Ray Analysis. Plenum Press, New York, 26-27.

[22] Niedrig H (1982) Electron backscattering from thin films. J. Appl. Phys. **53**, R15-R49.

[23] Niemietz A, Reimer L (1985) Digital image processing of multiple detector signals in scanning electron microscopy. Ultramicroscopy **16**, 161-174.

[24] Reimer L, Stelter D (1987) Monte Carlo calculations of electron emission at surface edges. Scanning Microscopy, **1**, 951-962.

[25] Robinson VNE (1980) Imaging with backscattered electrons in a scanning electron microscope. Scanning **3**, 15-26.

[26] Rosler M, Brauer W (1981) Theory of secondary electron emission. II. Application to aluminium. Phys. Stat. Sol. (b) **104**, 575-587.

[27] Seiler H (1967) Einige aktuelle Probleme der Sekundärelektronenemission. (Some actual problems concerning secondary electron emission.) Z. Angew. Phys. **22**, 249-263.

[28] Seiler H (1983) Secondary electron emission in the scanning electron microscope. J. Appl. Phys. **54**, R1-R18.

[29] Tholomier M, Vicario E, Doghmane N (1987) Simulation par la méthode de Monte Carlo de l'influence des électrons rétrodiffusés en spectrométrie d'électrons Auger. Ière partie. (Monte Carlo simulations of the influence of backscattered electrons on Auger electron spectrometry. First Part.) J. Microsc. Spectrosc. Electron. **12**, 449-460.

[30] Wells OC (1971) Low-loss image for surface scanning electron microscopy. Appl. Phys. Lett. **19**, 232-235.

[31] Wells OC (1972) Low-loss image formation in the surface SEM. Nat. Conf. El. Probe Microanalysis, San Francisco Press, 16A-16C.

Discussion with Reviewers

J. Hejna: Your equipment gives rather large beam diameter and relatively high acceleration voltages. Is it possible to improve these parameters in your electron optical configuration?

Authors: The smallest beam diameter (0.3 μm) that we could realize is pretty large, in fact. Numerous reasons exist for this. The primary electrons are accelerated to energies in the range between 50 and 100 keV. In order to accelerate the secondary electrons emerging from the specimen surface, it must be held on a negative potential of -30 kV. Consequently, the primary electrons are decelerated to energies of 20-70 keV before hitting the surface of the specimen. This requires rather complicated electron optics with a lot of compromises in many respects. We have a large working distance of 10 cm between the last demagnifying lens and the specimen and a decelerating lens in between. The decelerated electron probe has to cross the accelerating field of the cathode lens obliquely. The latter point mentioned prevents us from going to energies of less than 20 keV of the impinging primaries. Electrons with much less than 20 keV are strongly deflected by the high electric field in front of the specimen and do not reach the specimen. On the other hand, an electric field as high as possible in front of the specimen is desirable in order to achieve a high resolution of the cathode lens and, in turn, of our spatial distributions of the secondaries. With a 5 μm diaphragm and 50 kV/cm field strength and photoemitted electrons, which have a smaller energy width compared to secondary electrons, 10 nm of resolution of such a cathode lens has been achieved in emission microscopes dedicated for high resolution work. We could not reach these resolution values because we had to make some compromises: (**1**) we used a diaphragm with a diameter of 30 μm (which lowers the resolution compared to a 5 μm diaphragm) in order to achieve acceptable electron intensities; and (**2**) the distance between the specimen (cathode) and the Wehnelt-electrode of the cathode lens was chosen to be rather large in order to allow the primary electrons to hit the specimen. This results in a low field strength of only 20 kV/cm in front of the specimen and a further reduction in the resolution (about 100 nm) of our cathode lens. Having in mind that, e.g., the spatial extend of the distribution of secondaries released by a primary beam of 40 keV from a flat silicon specimen is about 20 μm in diameter, this modest resolution still gives us valuable information. The present configuration cannot be improved substantially by small changes.

J. Hejna: Is it possible to construct the instrument with a magnetic prism for separation of primary and emitted electrons as in the LEEM instrument of Telieps and Bauer? Such configuration would enable one to work with untilted specimens.

Authors: When this instrument was designed in the early seventies, this elegant solution was considered but

rejected. It seemed to be too complicated as a first step. We agree with you; the best configuration would be a field emission electron gun, a magnetic prism, a high resolution cathode lens and a channelplate image intensifier to intensify the emission micrograph. This micrograph should be transferred fiber optically to a state of the art slow scan CCD-camera-densitometer as described in this paper.

K. Murata: With your CCD-camera, how small of a beam current can you go to under a reasonable signal intensity? Generally, the smaller beam current you have, the smaller beam spot you can get.
Authors: There are two aspects that have to be considered: (1) Electron optics and current in the electron probe and (2) noise due to electron statistics and detection quantum efficiency of the CCD-camera. In our present setup, beam spots smaller than the resolution of the cathode lens (0.1 μm) make no sense. In an improved setup, as described in the answer to J. Hejna, a resolution of the cathode lens of 0.01 μm would be possible. In both cases, the great problem to be solved is how to get the highest possible beam current. In the present setup, we have a compromise between a large working distance, the beam spot size and the current in this spot. A system with 0.01 μm resolution will not work without a field emission cathode and an image intensifier. The current in the electron probe is crucial in our experiment, since we are not interested in the SE1 current density but in the spatial distribution of the SE2 current density which is smaller by at least two or three orders of magnitude. In the low-intensity SE2 distributions, electron statistics becomes very important. In fact, electron statistics is the limiting factor for the grey level resolution of the SE2 distributions and not the detection quantum efficiency of the CCD-camera (1 imaging electron of 20 keV produces 1700 photons of 560 nm in a P20 phoshor. Assuming a transfer rate of 40 % for photons to a CCD-pixel and a quantum yield of 40 %, about 250 electrons are generated in a pixel. This number is far beyond the noise level of the camera if we choose an integration time of some seconds and the sensor is cooled. In TV-mode, the noise level of the uncooled sensor is about 200 electrons).

K. Murata: Could you comment the fluctuations in the intensity on the flat region in Figure 6?
Authors: These fluctuations are the result of the so called "fixed pattern noise" which has two components: (1) dark signal non-uniformity and (2) photo response non-uniformity. In the spatial distributions presented in this paper, we did not correct these noise components. The distributions are densitometric evaluations of photographically recorded micrographs with the high intensity parts strongly overexposed. Therefore, in the photograph there are no intensity fluctuations in this region, i.e., the fluctuations in Figure 6 are due to photo response non-uniformities of our CCD-camera.

K. Murata: Is it possible to develop a more sensitive and high resolution detector by adding a multi-channel plate which is commercially available?
Authors: This proposal will be very interesting when a setup as described in the answer to J. Hejna is realized. In order to get a resolution of 10 nm of the emission microscope, the diameter of the diaphragm in the back focal plane of the cathode lens has to be reduced to 5 or 10 μm with a corresponding loss in intensity of at least a factor of 10. In addition, the current in the smaller primary probe (which is not possible in our actual setup) is a few orders of magnitude smaller. Ergo, in the present setup with a thermionic cathode, without image intensifying by, e.g., a multi-channel plate it would be absolutely impossible to see anything. To use a field emission cathode is mandatory when going to these high resolutions.

Z. Radzimski: What are the limitations of the optics of the electron emission microscope with respect to the energy of the entering electrons? How high of an energy can still be visualized without distortion? Can the geometry of the optic system be changed to investigate more realistic cases related to SEM, i.e., normal incidence angle and lower beam energy?
Authors: The larger the energy of the entering electrons, the less the deflection of the electrons and distortion of the electron probe on their path across the electric fields of the decelerating lens and that in front of the specimen surface. The energy of the impinging probe has no influence on the imaging characteristics of the cathode lens. The cathode lens exclusively uses the low-energy secondary electrons (0 to few eV) for imaging purposes. The diameter of the diaphragm in the back focal plane of the cathode lens determines the upper limit of the energy of the secondaries used to form the image. It works as a low-pass filter. Backscattered electrons do not contribute to the image at all.

Z. Radzimski: How was the parameter β determined in this work? Did you try to use a very thin self supporting layer to evaluate the SE1 component?
Authors: The two-dimensional spatial distribution of SE1 + SE2 consists of a narrow Gaussian peak of SE1 with a full width at half maximum corresponding to that of the impinging primary electron probe on the broad distribution of SE2, which is likewise of Gaussian shape according to our experiments. The parameter β was determined by integrating the intensity below the SE1 +

SE2 spatial distribution in two dimensions. The integration in the first dimension was achieved by deflecting the probe into a line and analyzing the density distribution perpendicular to this line. The densitometer trace across this line was composed by two Gaussian distributions corresponding to the SE1 and SE2 components. By evaluating the integrals below these distributions analytically, β was calculated [see ref. 12]. In a preliminary experiment, we measured the SE1 component according to your proposal by using a thin film specimen. The result was that the full widths at half maximum of SE1 distributions emerging from thick specimens did not differ from our observations on thin films within the error limits.